An efficient feedback control algorithm for beams: experimental investigations

Frédéric Bourquin, Michel Joly, Manuel Collet, Louis Ratier

An efficient feedback control algorithmfor beams: experimental investigations

F. Bourquin[a], M. Joly[a], M. Collet[b,*], L. Ratier[c]

[a] *Laboratoire Central des Ponts et Chaussées, and Laboratoire Lagrange, 58 boulevard Lefebvre, F 75732 Paris cedex 15, France*

[b] *Laboratoire de Mécanique Appliquée R. Chaléat, CNRS UMR 6604, 24 chemin de l'Epitaphe, 25000 Besancon, France*

[c] *LM2S, CNRS UMR 6604, Université Pierre et Marie Curie, Ecole Normale Supérieure de Cachan, Laboratoire Central des Ponts et Chaussées and EDF, Paris, France*

An experimental implementation of a rapid active control strategy for flexible structures combined with a modal filter for state reconstruction is presented. The control law, which builds upon Komornik's original idea, is designed so as to achieve an arbitrarily large decay rate of the energy of the system, at the price of solving once and for all a well-conditioned small-size linear system, instead of a Riccati equation. It is applied to a slender beam. The fundamental ideas and properties of this simple but efficient strategy are explained. The emphasis is put on the practical implementation and on the experimental results, which show an important increase of the apparent modal damping even for values of the resulting gain that do not generate spill-over. The proposed feedback outperforms the standard LQ control. The actual behaviour of the closed-loop system is accurately predicted by a complete electro-mechanical model that accounts for the identified dynamics of the shaker.

1. Introduction

There exist various strategies to control the vibrations of structures: the simplest one is probably the direct velocity feedback [1] that can also be implemented as the integral force feedback [2,3]. This collocated approach does not rely on any model, and in principle does not generate spill-over, but may lack efficiency due to the spatial localization of the damping effect and to the necessary low- or high-pass filtering which strongly deteriorates the performances at high or low frequencies. Moreover, spill-over shows up in practice due to the difficulty to achieve

*Corresponding author.
E-mail address: manuel.collet@univ.fcomte.fr (M. Collet).

collocation, and due to sensor or actuator dynamics. Another usually non-collocated approach is the classical LQ strategy and multiple variants, which are a priori more efficient and insure global stabilization, provided that controllability hold [4–8]. Nevertheless, a state space model is required for implementation purposes, and its necessary finite-dimensional approximation may give rise to spill-over instabilities [9].

Following the earlier works of Lions [10] on the exact controllability of partial differential equations, Komornik has introduced an efficient and simple strategy to stabilize flexible structures [11,12]. His method assumes the exact controllability of the structure to hold at the continuous level. This property depends on the mechanics of the structure and of the geometry, see e.g. Refs. [10,13–20].

Whenever the exact controllability of the structure holds, a control law based on the inversion of a modified controllability gramian [11,12] leads to a uniform decay rate of the total energy which is larger than ω where the parameter ω can be arbitrarily chosen in the design of the control law. Therefore, this control law can be as efficient as one wants in the sense that some suitable norm of the state is bounded by $C(\omega)e^{-\omega t}$ at any time t. Moreover this property holds uniformly with the modal discretization [21]. This control algorithm behaves as a pole placement algorithm, although the poles of the closed-loop system are not specified during the control synthesis. Recall that it is not easy to predict the decay rate of the energy of the closed-loop system for a given control law [12,22,23]. In general the rate at which the energy decays cannot be larger than some *critical damping* that depends on the structure [3].

Therefore the most striking feature of Komornik's control strategy is certainly the possibility for the user to prescribe the resulting decay rate and to handle it as the *unique design parameter* during the control synthesis.

Moreover, the control strategy can be implemented on-line in a simple way and, in particular, does not require the solution of any Riccati equation, contrary to the standard LQ strategy. It only requires to solve a simple linear system. On the other hand, a smoothed version of this control strategy enables one to reduce the possible control spill-over [24]. See Refs. [24–27] for computational aspects and variants of the original law.

This contribution aims at assessing experimentally the efficiency of Komornik's feedback per se and in comparison with the classical LQ strategy. The experimental results enhance previous ones [28]. Moreover, the role of the actuator in the global closed-loop dynamics is analyzed. The control system imposes the displacement at one endpoint of a simply supported beam [29].

This paper is organized as follows: Section 2 contains background information on the proposed control strategy at the continuous level. The experimental setting is presented in Section 3. The identification technique of the modal filter which helps reconstructing the state of the system is detailed in the Appendix. An approximation of the feedback law is introduced in view of on-line computations, and a similar framework is developed for the LQ feedback. Experimental results regarding white noise and impulse disturbances are presented in Section 4. In both cases the proposed strategy proves efficient to control the first modes of the system. The relative advantages of LQ, IFF, and Komornik's strategies are also discussed. Then, in Section 5, the experimental results are analyzed by means of a complete electro-mechanical model that takes into account the actuator behaviour. This approach enables one to explain the practical limitations of the proposed control strategy in terms of the largest value of the parameter ω preventing the closed-loop system from instabilities.

2. Komornik's feedback law

Consider a simply supported Euler–Navier–Bernoulli beam of length L. Let ρ, E, A, I denote its mass density, Young's modulus, cross-sectional area and inertia respectively. For the sake of simplicity, the mass density per unit length ρA and the stiffness EI are supposed to be constant along the beam. Moreover, damping is not taken into account, mostly because the real beam that has been investigated proves very lightly damped as shown in Table 1. Civil engineering structures such as cables enjoy the same property. Even large structures like bridges may have no damping or a negative damping because of wind–structure interaction. Therefore it seems fair to design control laws without damping and to test them on slightly damped or undamped structures. But introducing damping in the equations is possible from the theoretical point of view [30], provided observability holds and the damping is not too large. It is shown that positive or negative destabilizing damping can be overcome by a controller of the type described below, provided the parameter ω is large enough. Note that positive damping may not enhance the performance of the controller.

Thus the transverse displacement $y(x,t)$ satisfies

$$\begin{cases} \rho A \partial_{tt} y(x,t) + EI \partial_{xxxx} y(x,t) = 0, & [0,L] \times [0,T], \\ y(0,t) = v(t), & [0,T], \\ y(L,t) = \partial_{xx} y(0,t) = \partial_{xx} y(L,t) = 0, & [0,T], \\ y(x,0) = y^0(x), \partial_t y(x,0) = y^1(x), & [0,L]. \end{cases} \tag{1}$$

Here the beam is controlled through the imposed transverse displacement at the left endpoint, although other types of actuation can be considered as well, and the control horizon T can be arbitrarily large. In order to design the state feedback law $v(t) = \mathscr{F}(y(t), \partial_t y(t))$, an adjoint state is introduced : let $\varphi(x,s)$ denote the unique solution of the beam equation

$$\begin{cases} \rho A \partial_{ss} \varphi(x,s) + EI \partial_{xxxx} \varphi(x,s) = 0, & [0,L] \times [0,S], \\ \varphi(0,s) = \varphi(L,s) = \partial_{xx} \varphi(0,s) = \partial_{xx} \varphi(L,s) = 0, & [0,S], \\ \varphi(x,0) = \varphi^0(x), \partial_s \varphi(x,0) = \varphi^1(x), & [0,L], \end{cases} \tag{2}$$

where s denotes a fictitious time, and S a fictitious time horizon. The displacement field φ depends linearly on the initial conditions $\{\varphi^0, \varphi^1\}$. Hence, for any value of ω one can define the modified bilinear controllability gramian

$$a_{\omega,S}(\{\varphi^0, \varphi^1\}, \{\hat{\varphi}^0, \hat{\varphi}^1\}) = \int_0^S \mathrm{e}^{-2\omega s} EI \partial_{xxx} \varphi(0,s) EI \partial_{xxx} \hat{\varphi}(0,s) \, \mathrm{d}s, \tag{3}$$

Table 1
Modal parameters of the initial set-up

	Natural frequencies ω_i (Hz)	Damping ratios ξ_i (%)
Mode 1	3.0	0.09
Mode 2	10.8	0.06
Mode 3	23.7	0.1

where $\hat{\varphi}$ denotes the solution of (2) with initial conditions $\{\hat{\varphi}^0, \hat{\varphi}^1\}$. The function $e^{-2\omega s}$ initially introduced by Komornik [11] has to be slightly modified in view of the theory [12]. But from the numerical point of view, both choices yield similar results. Therefore the function $e^{-2\omega s}$ is kept.

Following e.g. Lebeau [15] it can be proved that for any smooth enough displacement and velocity fields z^0 and z^1, there exists a unique solution $\{\varphi^0, \varphi^1\}$ of the variational equation

$$a_{\omega,S}(\{\varphi^0, \varphi^1\}, \{\hat{\varphi}^0, \hat{\varphi}^1\}) = \int_0^L \rho A(z^1\hat{\varphi}^0 - z^0\hat{\varphi}^1)\,\mathrm{d}x \quad \forall\{\hat{\varphi}^0, \hat{\varphi}^1\}. \tag{4}$$

Let $\mathscr{L}_{\omega,S}$ denote the operator defined by $\{\varphi^0, \varphi^1\} = \mathscr{L}_{\omega,S}\{z^0, z^1\}$ and P_1: $\mathbb{R}^2 \to \mathbb{R}$ the projection on the first component, i.e. $P_1(\{a, b\}) = a$. The proposed feedback reads

$$v(t) = -EI\partial_{xxx}(P_1\mathscr{L}_{\omega,S}\{y(t), y'(t)\})(x = 0). \tag{5}$$

It is not obvious that the resulting system of equations is well-posed. Nevertheless, global existence of a unique solution is proved in [12] for the wave and the thin plate equations, as well as the decay estimate for the state of the closed-loop system

$$\|\{y(t), y'(t)\}\|_w \leqslant Ce^{-\omega t}\|\{y^0, y^1\}\|_w \tag{6}$$

for some constant C, where $\|\ \|_w$ stands for a suitable norm of the state, called the *w-norm* in the sequel. This *w-norm* puts the emphasis on the low-frequency content of the state and underweights the high-frequency components. The constant C depends exponentially on ω [31]. Numerous numerical tests show that the *w-energy*, i.e. the square of the *w-norm*, decays exactly as $e^{-4\omega t}$ for $S = +\infty$ [31]. This conjecture has been proved in Ref. [30].

• Of course, there is no reason why $y^0(x = 0) = v(t = 0)$ although this condition would be requested for compatibility. Numerical tests show that this condition is almost never satisfied if the control is computed as above. However the response of the structure is well defined in a "very weak" sense. Locally very strong stresses that may develop, can thus be smeared by smoothing techniques [24]. The actuator dynamics may also play the same role.

• It turns out [12] that this feedback law is nothing but a particular *optimal control* strategy associated with the quadratic cost functional

$$\mathscr{J}(y, v) = \int_0^{+\infty} (2\omega\langle\, \mathscr{L}_{\omega,S}\{y, \partial_t y\}, \{\partial_t y, -y\}\,\rangle + v^2(t))\,\mathrm{d}t, \tag{7}$$

where $\langle\, \{\psi^0, \psi^1\}, \{\eta^0, \eta^1\}\,\rangle = \int_0^L(\psi^0(x)\eta^0(x) + \psi^1(x)\eta^1(x))\,\mathrm{d}x$: The control $v(t)$ and the state $y(t)$, subject to (1), minimize the functional $\mathscr{J}(y, v)$. After a modal discretization, the functional to be minimized reads

$$\mathscr{J}^N(x, v) = \int_0^{+\infty} (2\omega x^t(t)Qx(t) + v^2(t))\,\mathrm{d}t, \tag{8}$$

where the matrix Q exhibits the non-intuitive structure displayed in Eq. (9) in the case of the beam described in the next section and discretized by means of the first three modes:

$$Q = \begin{bmatrix} 1.9238 & -0.0003 & -0.0001 & 0.1120 & 0.0149 & 0.0019 \\ -0.0003 & 0.0300 & -0.0000 & -0.0037 & 0.0004 & 0.0003 \\ -0.0001 & -0.0000 & 0.0026 & -0.0002 & -0.0001 & 0.0000 \\ 0.1120 & -0.0037 & -0.0002 & 1.9285 & 0.0006 & 0.0001 \\ 0.0149 & 0.0004 & -0.0001 & 0.0006 & 0.0301 & 0.0000 \\ 0.0019 & 0.0003 & 0.0000 & 0.0001 & 0.0000 & 0.0026 \end{bmatrix}. \tag{9}$$

• Some earlier works [32] contain a restricted version of this feedback, namely the case when $\omega = 0$. There is also a clear connection with receding horizon control [33] since an exact controllability problem in open loop is solved at every time t and the resulting control is applied over the next "sampling step" when it comes to real-time implementation.

• The full generality of the approach is not questionable since it can be developed in the case of an abstract dynamical system in state-space form

$$\dot{x} = Ax + Bu, \quad x(0) = x_0. \tag{10}$$

In this setting, the modified controllability gramian (3) reads:

$$a_{\omega,S}(\varphi, \psi) = \int_0^S \mathrm{e}^{-2\omega s}(B^* \mathrm{e}^{A^* s}\varphi)(B^* \mathrm{e}^{A^* s}\psi)\,\mathrm{d}s. \tag{11}$$

If the strong observability inequality $\int_0^T (B^* \mathrm{e}^{A^* t}\psi\,\mathrm{d}t)^2\,\mathrm{d}t \geqslant \alpha|\psi|^2$, basic to the Hilbert Uniqueness Method (HUM) [10], holds for some T and some positive α, then for S large enough the operator $\Lambda_{\omega,S}$ defined by $\langle \Lambda_{\omega,S}\varphi, \psi \rangle = a_{\omega,S}(\varphi, \psi)$ for the natural duality product $\langle .,. \rangle$ is invertible. Define $u(t) = B^* \Lambda_{\omega,S}^{-1} x(t)$, then [12] $\|x(t)\| \leqslant C\mathrm{e}^{-\omega t}\|x_0\|$.

The observability inequality cannot be proved in the abstract setting and the physics of the system must be taken into account. In the same way, convergent and fairly general methods of approximation are based on the mechanical understanding of the main quantities involved [26,27,34–37]. This is part of why a concrete pde-based approach seems useful.

As a conclusion, the control law defined in Eq. (5) induces a *prescribed decay rate* of some norm of the system according to estimate (6). The feedback gain results from solving a small-scale linear system of equations, associated with a symmetric positive definite matrix, with no need of solving any Riccati equation. In the case of a general, possibly damped, structure, the observability condition still must be satisfied in view of positive definiteness. Besides, it is usually advocated to assert the well-posedness of the infinite horizon LQ regulation problem. Therefore Komornik's feedback essentially applies in the same conditions as infinite horizon LQ regulator. Computational details are to be found in Refs. [24–26,31].

An experimental implementation of this method is presented in the next section.

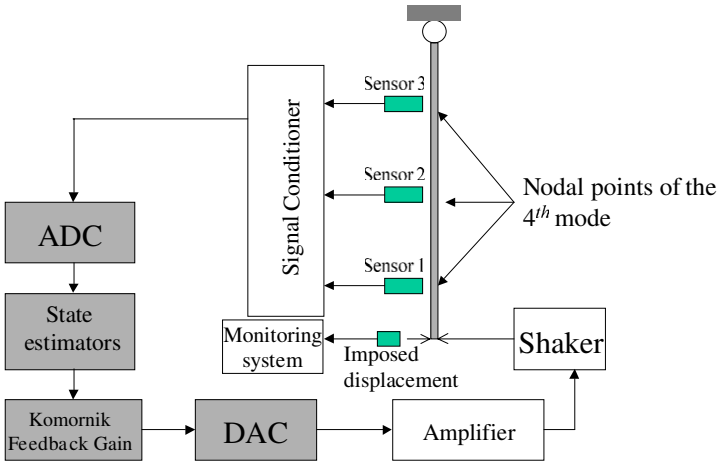

Fig. 1. Experimental set-up.

3. Experimental setting

The structure of interest is a simply supported steel beam of the following dimensions: length $L = 1870$ mm, width $l = 40$ mm, and thickness $h = 4$ mm (Fig. 1). The boundary conditions are obtained by well-suited mechanical connections: a ball joint at the top and a pinching at the bottom. As shown in Fig. 16, the electro-mechanical actuator and its amplifier enable one to impose quasi-proportional structural displacements in a frequency range of 1 to 40 Hz, which includes the first three modes. That the upper bound of this range coincides with the fourth eigenfrequency of the structure is a matter of pure chance. The shaker has not been tuned but rather used as is. The control feedback is computed by a 60 MHz Texas Instrument © DSP TMS320C31 DSP. All the programming procedures build upon Matlab-Simulink © tools and fit in this environment. In order to minimize if not eliminate from the measured displacements the contribution of mode 4, whose natural frequency is 41 Hz, the sensors are placed at the theoretically predicted nodes of mode 4. In this configuration, this mode cannot contribute to the observation spill-over provided the theoretical or numerical placement coincide with the real one. This kind of strategy was proposed among others in Refs. [38–40]. The main aim here is to experimentally prove the efficiency of the simple boundary control strategy presented in the last section. Above treatment of spill-over proves sufficient to achieve this goal since experiments match theory. Therefore, no special effort has been dedicated to enhance this treatment of spill-over.

3.1. State estimation

In this section, the mode shapes of the simply supported beam at both ends are assumed to be known. Attention is paid here to the estimation of the generalized modal co-ordinates. The identification of the mode shapes will be detailed in the next subsection. The deflection of the beam is only known at the three sensor locations. Then, in order to compute the feedback gain (5) and to implement the strategy on the beam, a finite modal decomposition of the displacement is useful. Let $(\lambda_i, \theta_i)_{i=1}^{+\infty}$ denote the family of eigenvalues and normal modes of the simply supported

beam (when $y(0,t)=0$). The modes are assumed to be normalized so that they have a unit mass. The displacement all over the beam is decomposed by mode superposition as follows:

$$y(x,t)=\sum_{i=1}^{+\infty}\alpha_i(t)\theta_i(x). \tag{12}$$

This decomposition seems to contradict the actuation at one end, since a displacement is imposed but the modes vanish at that point. However this decomposition holds in a weak sense and works practically. The static mode is implicitly accounted for in the decomposition, by means of the Fourier coefficients $\alpha_i(t)$.

If M sensors located at $(x_k)_{k=1}^{M}$ are available, the displacement at each sensor location x_k satisfies, at least formally (see remark below)

$$\begin{bmatrix} y(x_1,t)\\ \vdots\\ y(x_k,t)\\ \vdots\\ y(x_M,t)\end{bmatrix}=\mathbf{C_d}\begin{bmatrix}\alpha_1(t)\\ \vdots\\ \alpha_k(t)\\ \vdots\\ \alpha_M(t)\end{bmatrix}+\sum_{i=M+1}^{+\infty}\alpha_i(t)\begin{bmatrix}\theta_i(x_1)\\ \vdots\\ \theta_i(x_k)\\ \vdots\\ \theta_i(x_M)\end{bmatrix} \tag{13}$$

where $\mathbf{C_d}(k,i)=\theta_i(x_k)$ is the general term of the modal participation matrix $\mathbf{C_d}\in\mathbb{R}^{M\times M}$. Thus, whenever the matrix $\mathbf{C_d}$ is non-singular, an estimation $[\bar{\boldsymbol{\alpha}}]_M$ of the true modal intensities $[\boldsymbol{\alpha}]_M$ of the first M modes can be defined as follows:

$$\begin{aligned}[\bar{\boldsymbol{\alpha}}(t)]_M&=\mathbf{C_d}^{-1}[\mathbf{y}(\mathbf{x}_k,t)]_M\\ &=[\boldsymbol{\alpha}(t)]_M+\sum_{i=M+1}^{+\infty}\alpha_i(t)\mathbf{C_d}^{-1}\begin{bmatrix}\theta_i(x_1)\\ \vdots\\ \theta_i(x_k)\\ \vdots\\ \theta_i(x_M)\end{bmatrix},\end{aligned} \tag{14}$$

where $[\mathbf{y}(\mathbf{x}_k,t)]_M$ stands for the vector $(y(x_1,t),\ldots,y(x_k,t),\ldots,y(x_M,t))'$. The online estimation of the modal intensity vector $[\boldsymbol{\alpha}]_M$ is thus based on the outputs of the sensors using the classical modal filter $[Filter]_{M\times M}=\mathbf{C_d}^{-1}$. See Refs. [38,39] for various properties of this method and some sensor optimization based solutions to the problem of the spill-over introduced by the residual term in Eq. (14), in view of enhancing the control efficiency.

Remark. (i) The series expansion (12) may not converge pointwise in space. Therefore, Eq. (13) and the second line of Eq. (14) may not make sense but highlight the reason of observation spill-over in this context. However, the first line of Eq. (14) does make sense, and this is all that is needed in order to develop the rest of the control procedure.

(ii) If N modes were to be controlled with $N>M$ then a state reconstruction, e.g. a Kalman filter or a Luenberger observer, would be needed.

In view of the control synthesis, the so-called modelled dynamics will be spanned by the first $N=M$ modes of the beam. The largest possible number of modes will then be controlled. The

velocities are assumed here to be reconstructed by numerical derivation and filtering of the measured displacements. The beam transverse displacement is estimated here by only keeping in Eq. (12) the modes whose participation has been estimated:

$$\bar{y}_N(t,x) = \sum_{i=1}^{N} \bar{\alpha}_i(t)\theta_i(x) \;\; \partial_t \bar{y}_N(t,x) = \sum_{i=1}^{N} \overline{\partial_t \bar{\alpha} i}, \tag{15}$$

where $\overline{\partial_t \bar{\alpha}_i}(t)$ stands for a numerical time derivative of $\bar{\alpha}_i(t)$, realized by means of a specific second order low-pass derivative filter.

3.2. *Modal filter identification*

The mode shapes of an ideal simply supported Euler–Navier–Bernoulli beam are well known. However, they are not exactly similar to the experimentally observed ones because of imperfect boundary conditions, error in the material characteristics or in the dimension of the system. Therefore the modes shapes must be identified.

The modal parameters of the beam and, above all, the terms $[\theta_i(x_k)]_{i,k=1,\ldots,3}$, basic to the expression of the modal filter, have been obtained by means of an impulse testing method relying on a hammer with incorporated force sensor [41,42]. After curve fitting, poles and residues are computed from the transfer functions between the measured displacements and the impulse load. These experimental transfer functions and corresponding fitting curves are shown in Figs. 2–4. As expected the fourth mode is not measured by the sensors. On the other hand, the second sensor does not pick up the modal intensity of the second mode because it measures the displacement at the middle of the beam. Within the 0–40 Hz bandwidth, the first three eigenfrequencies and the

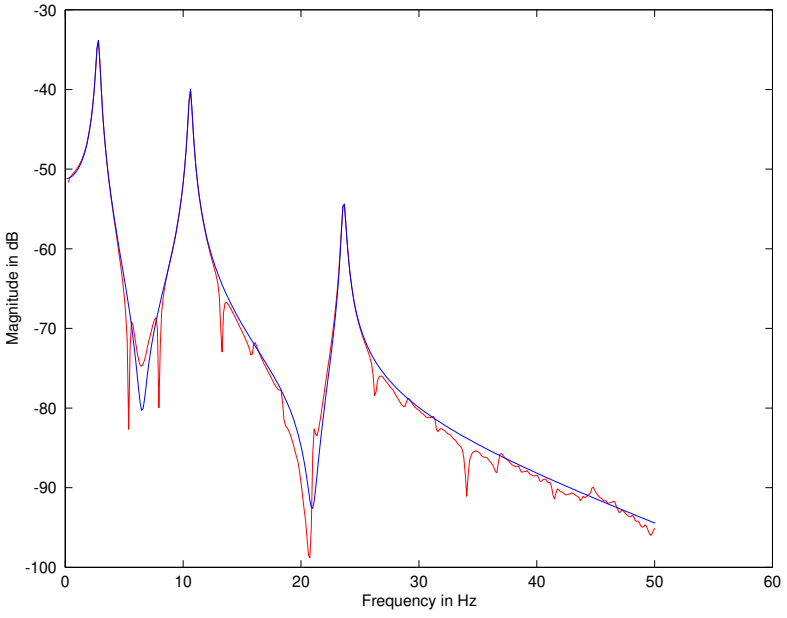

Fig. 2. Experimental transfer function (..) and the fitted curve (-) of sensor 1.

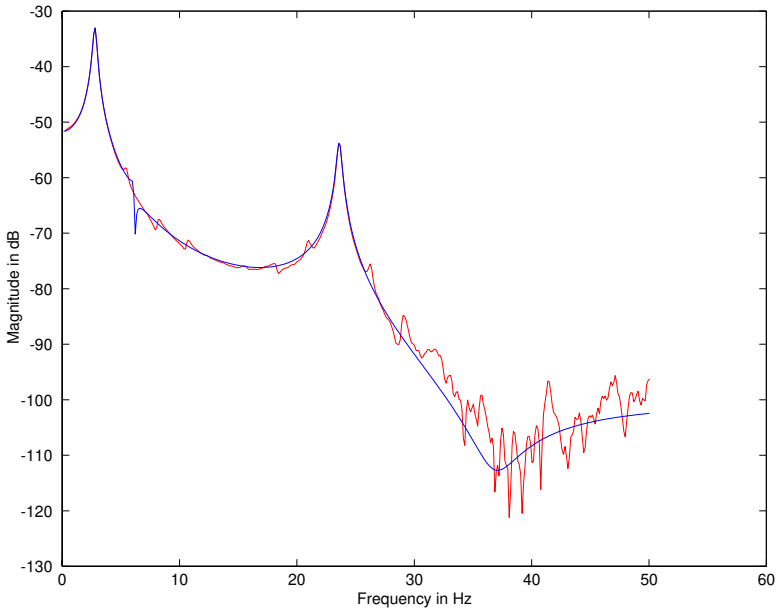

Fig. 3. Experimental transfer function (..) and the fitted curve (-) of sensor 2.

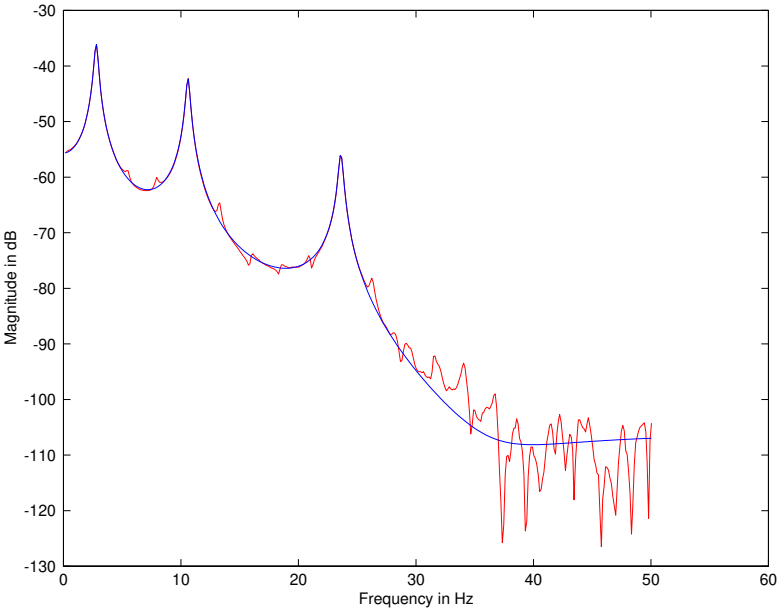

Fig. 4. Experimental transfer function (..) and the fitted curve (-) of sensor 3.

associated modal damping ratios are identified and given in Table 1. Only the corresponding modal intensities are considered to compute the control by using relations (15) in Eq. (5).

The quality of the filtered signal, which will be used as a modal estimator in the control feedback, is shown in Figs. 5–7. In the frequency band of interest (0–40 Hz), the modal estimators

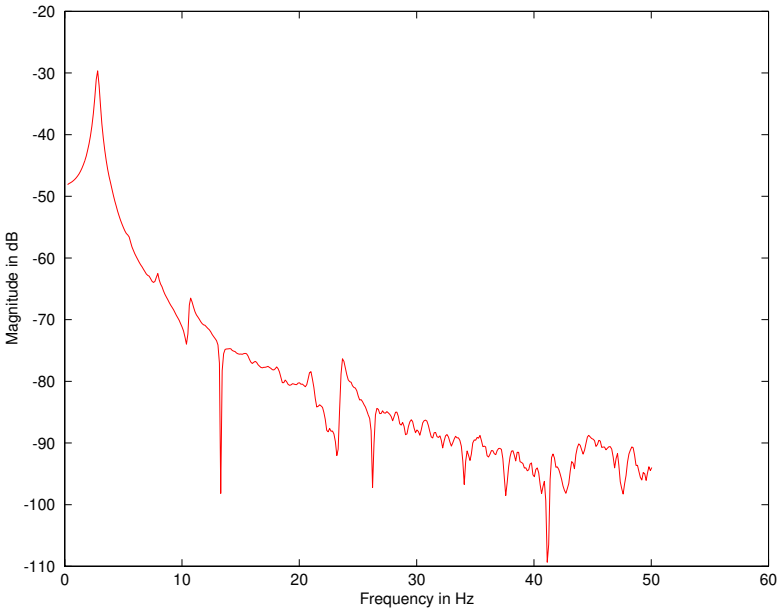

Fig. 5. FRF of the first mode estimator signal.

are good enough to be used in the control feedback. The modal signal corresponding to the third mode is not really uncoupled from the first two because of difficulties in reaching sufficient accuracy when estimating the modal parameters from the sensors. These difficulties may come from signal processing parameters, sensor non-linearities, or boundary conditions. Nevertheless, the first observed residual mode at 68 Hz is far enough from the frequency band of interest to be filtered by a classical temporal low-pass filter which has been implemented together with the feedback itself. In this way, the risk of spill-over instabilities is partly mitigated.

3.3. *Real-time approximation of the control law*

Table 1 confirms the small damping assumption. This justifies the equations displayed in Section 2. From now on, damping is neglected in the elastodynamic equations used for the design of the control laws that are tested in this paper.

Let V_N denote the space spanned by the first N modes θ_i of the simply supported beam. In order to compute a control with the discrete estimated state $(\bar{y}_N(t,x), \hat{\partial}_t \bar{y}_N(t,x))$, the bi-linear controllability gramian (3) is projected over $V_N \times V_N$: for every pair of functions $\{z^0, z^1\}$, define $\{\varphi_N^0, \varphi_N^1\} \in V_N \times V_N$ as the solution of the variational equation

$$a_{\omega,S}(\{\varphi_N^0, \varphi_N^1\}, \{\hat{\varphi}_N^0, \hat{\varphi}_N^1\}) = \int_0^L \rho A(z^1 \hat{\varphi}_N^0 - z^0 \hat{\varphi}_N^1)\,\mathrm{d}x \quad \forall \{\hat{\varphi}_N^0, \hat{\varphi}_N^1\} \in V_N \times V_N \tag{16}$$

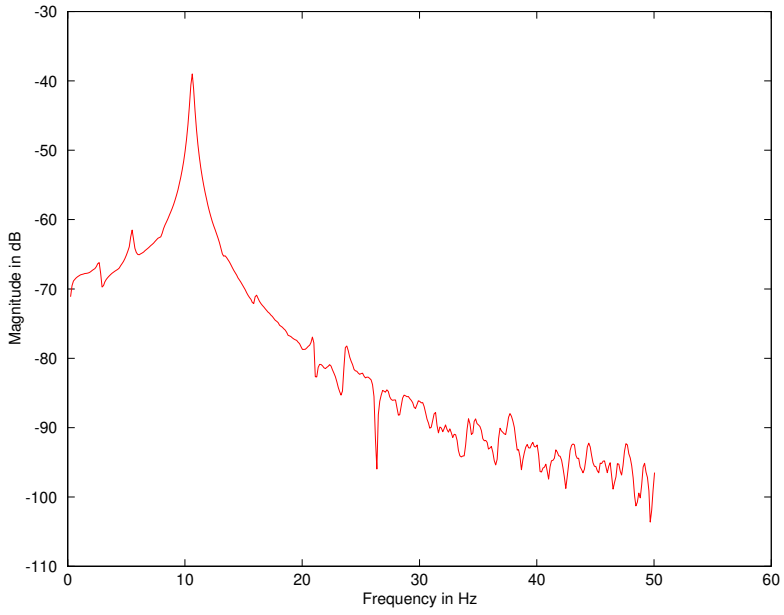

Fig. 6. FRF of the second mode estimator signal.

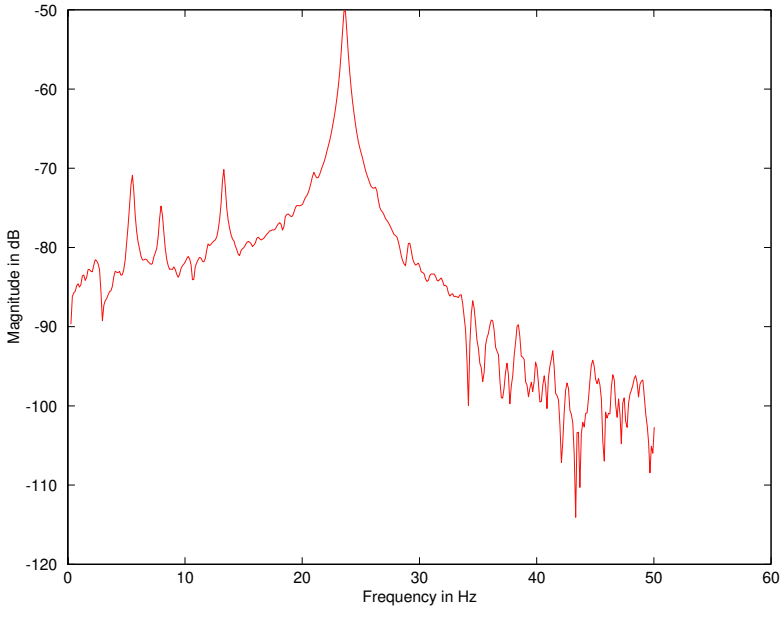

Fig. 7. FRF of the third mode estimator signal.

and set $\varphi_N^0 = \mathscr{L}_N\{z^0, z^1\}$. In the same way as in the continuous case, the control is defined as: $v_N(t) = -EI\partial_{xxx}\mathscr{L}_N\{\bar{y}_N(t), \overline{\partial_t \bar{y}_N}(t)\}(x = 0)$, or equivalently in matrix form:

$$v_N(t) = -[\mathbf{T}]_N[\mathbf{K}]_{N\times 2N}[[\bar{\alpha}]_N(t),\ \overline{\partial_t[\bar{\alpha}]_N}(t)]^t, \tag{17}$$

where $[\mathbf{T}]_N = [t_1, \ldots, t_N]$, and $t_i = EI\partial_{xxx}\theta_i(x=0)$ stands for the end shear force of the ith mode of the reference model (1) with $v(t) = 0$, and $\mathbf{K}$ represents the matrix associated to $\mathscr{L}_{\mathscr{N}}$, the computation of which is detailed in Refs. [29,31]. Note that $\mathbf{K}$ depends on ω, S and $[\mathbf{T}]_N$. Here the first three modal participations are estimated and $N = 3$. Thus, it is now possible to test the efficiency of above feedback law, per se, but also in comparison with the classical LQ feedback.

3.4. LQ implementation

The same mechanical system with the same actuator is used for the implementation of the LQ strategy. Therefore the state equation must accomodate for displacement controls. In order to describe the dynamics of the system, a "spatially very weak" formulation of the beam equation is introduced as in Refs. [25,26,31]. Formal integrations by parts of (1) after multiplication by a smooth displacement field w lead to the formulation:

For all $w(x)$ smooth enough such that $w(0) = w(L) = \partial^2 w(0)/\partial x^2 = \partial^2 w(L)/\partial x^2 = 0$:

$$\int_0^L \rho A \frac{\partial^2 y}{\partial t^2}(x,t) w(x)\,\mathrm{d}x + EI \int_0^L y(x,t)\frac{\partial^4 w}{\partial x^4}(x)\,\mathrm{d}x + EIv(t)\frac{\partial^3 w}{\partial x^3}(0) = 0. \tag{18}$$

This equation is supplemented with initial conditions. An approximation $y_N(x,t)$ in V_N of the displacement y is defined as the solution of Eq. (18) with $w \in V_N$. The N resulting equations can be written in a state space form:

$$\begin{cases} \dot{\mathbf{X}}(t) = [\mathbf{A}]\,\mathbf{X}(t) + [\mathbf{B}]\,\mathbf{v}_N(t), \\ \mathbf{X} = [\bar{\boldsymbol{\beta}}_N(t),\ \partial_t \bar{\boldsymbol{\beta}}_N(t)]^t \end{cases} \tag{19}$$

with initial conditions $[\boldsymbol{\beta}_N(0)]_i = \int_0^L \rho A y^0(x)\theta_i(x)\,\mathrm{d}x, [\partial_t \beta_N(0)]_i = \int_0^L \rho A y^1(x)\theta_i(x)\,\mathrm{d}x$. The LQ regulator results from minimizing the cost functional: $\mathscr{J}(X,v) = \int_0^{+\infty} X^{\mathrm{T}}[Q]X + \mathbf{v}^{\mathrm{T}}\mathbf{R}\mathbf{v}\,\mathrm{d}t$, over all $\mathbf{v}$ and $\mathbf{X}$ satisfying Eq. (19). Here $\mathbf{Q} = \begin{bmatrix} diag(\lambda_i) & 0 \\ 0 & I \end{bmatrix}$ and $\mathbf{R} = r\mathbf{I}$ in order to minimize the mechanical energy. Note that r has been decreased as much as possible during the experiment in order to maximize the control efficiency while still avoiding the spill-over instability. As usual, this minimization leads to the resolution of an algebraic Riccati equation, that has been solved with Matlab.

Notice that even if the way the control is designed is different for Komornik's and LQ feedbacks, the resulting control equations are similar in the sense that, for each strategy, $\mathbf{v}_N(t) = -[\mathbf{G}]_N[[\bar{\boldsymbol{\beta}}]_N(t), \partial_t[\bar{\boldsymbol{\beta}}]_N(t)]^t$, where $[\bar{\boldsymbol{\beta}}]_N$ stands for a real-time estimation of $[\boldsymbol{\beta}]_N$, and similarly for the time derivatives. This estimation is carried out by means of the modal filter described in Section 3, in order to compare the feedback laws with the same state estimator.

Remark. (i) the choice of the weighting matrix $\mathbf{Q}$ refers to the minimization of the total energy at the discrete level, whereas this quantity is too strong a norm to be defined since a boundary displacement is imposed. A matrix corresponding to a weak norm should be introduced, in view of the continuous case. However, at the discrete level, all choices are possible, therefore the above choice is made in view of comparing the proposed algorithm with standard ones.

(ii) Although optimal in some sense, Kalman filtering proved much less efficient than modal filtering in view of stabilizing the beam, probably because it needs some time to reconstruct the true dynamics of the beam. But in the case of a sudden external load, allowing some time for state

reconstruction before controlling would clearly result in a poor efficiency. In this case, a preliminary and continuous training of the Kalman filter might be of interest.

4. Experimental results

Two different disturbances are considered: a white Gaussian noise in view of testing disturbance rejection, and an impact to highlight the stability of the controlled system.

It is noteworthy to emphasize that both disturbances are applied far from the actuator, with a coil or a hammer. Generally speaking, excellent results might be obtained with classical control laws when the actuator is located very close to the point where the disturbance is applied. In practice, wind- and earthquake loads may be considered as distributed, at least in a frame attached to the moving ground.

4.1. Komornik's feedback with exogeneous white noise disturbance

A white Gaussian force is applied via a field coil fixed at the 3/4th of the length of the beam. The feedback control starts after 8 s of recording. The control parameters chosen in the algorithm are $\omega = 1$, $S = 30$ s. The displacement imposed by the actuator is presented on the bottom left curve of Fig. 8, while the other three curves above (Fig. 8 left) show the displacement at the sensor locations that is to say at 1/4, 1/2, 3/4 of the length of the beam. The corresponding modal intensities estimated with the modal filter are shown in Fig. 8 on the right. Only the first two modes are well stabilized.

The *w-energy* is computed from the experimental results. Let $\bar{y}_N(x,t)$ denote the estimated displacement as in Eq. (15). It only contains the flexible components of the movement and no term takes into account the static displacement imposed by $v(t)$. Then [31]

$$\|\bar{y}_N(t), \bar{y}'_N(t)\|_w^2 = \sum_{i=1}^{N} \frac{\bar{\alpha}_i^2(t)L^2}{\rho A i^2 \pi^2} + \sum_{i=1}^{N} \frac{(\mathrm{d}\bar{\alpha}_i(t)/\mathrm{d}t)^2 L^6}{\rho A i^6 \pi^6}.$$

For a white noise disturbance, a -15 dB decrease can be observed on the *w-energy*, with $\omega = 1$, and $S = 30$ s (Fig. 9).

4.2. Komornik's feedback with exogeneous impulse disturbance

In this section, an impact is applied to the beam with a hammer. The frequency range which is actually excited by this perturbation includes the frequency band of interest. The corresponding energy (the power spectral density) is constant over the whole frequency band. The displacements are being recorded during 10 s. The impact is given at 0.1 s after the beginning of the recording, therefore the reference position is estimated during the first 0.1 s. Fig. 10 shows the imposed control and resulting displacement at sensors 1,2 and 3 with $\omega = 1$, $S = 30$ s on the right-hand side. The same displacements in the uncontrolled case are shown on the left of the same figure. The modal intensities computed with the modal filter are shown in Fig. 11, with $\omega = 1$ on the left and $\omega = 2$ on the right. As expected, the larger ω, the faster the decay of the response.

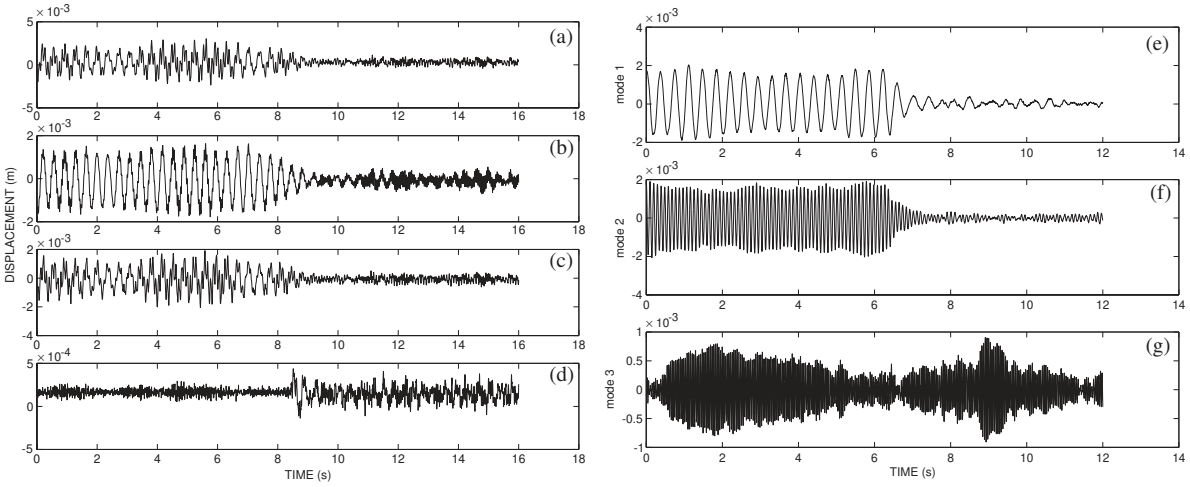

Fig. 8. Left (top-down): the displacements measured by sensors 1(a), 2(b), 3(c) then the controlling displacement (d), right: displacements modal intensities mode 1 (e), mode 2 (f), mode 3 (g); with white noise excitation, without control, and with control, $\omega = 1$, $S = 30$ s.

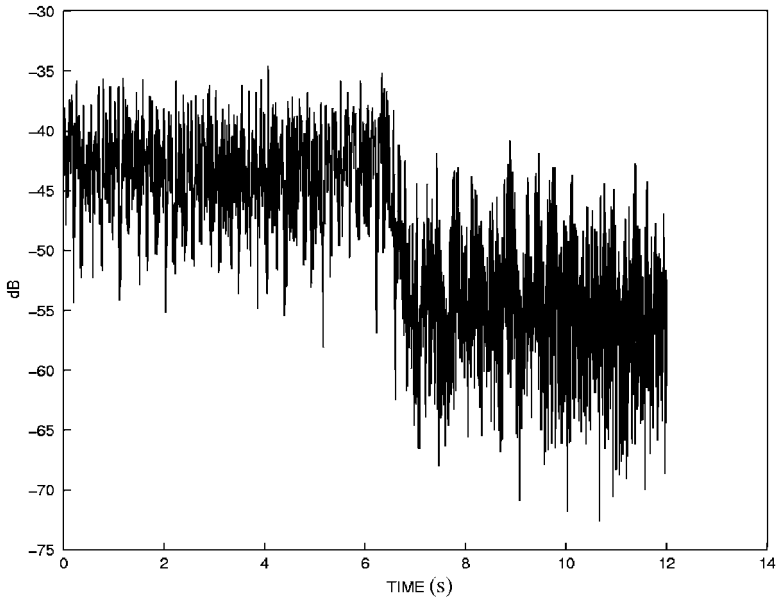

Fig. 9. *w-energy* of the structure, with white noise excitation, control starting at $t = 6.5$ s, $\omega = 1$, $S = 30$ s.

The modal damping ratios of the controlled displacements are estimated and shown in Table 2, which shows a dramatic improvement with respect to the uncontrolled case (Table 1).

It turns out that Komornik's strategy is very efficient to stabilize the first two modes. The damping ratios are very important compared with other algorithms. It is noteworthy to notice that experiments match simulations that rely on the spatially very weak formulation (18) [25,31].

However the stabilization of the third mode is not increased when the control changes from $\omega = 1$ to 2. In fact, the third natural frequency is quite close to the cutting frequency of the actuator (see Fig. 16). So, a coupling effect between the actuator and the mechanical system occurs explaining that the third mode is not very well controlled. An instability even appears on this degree of freedom when the parameter ω is larger than 2.2. The analysis of this phenomenum is presented in Section 4. The *w-energy* is shown in Fig. 12 in the impulse case for different values of the parameters ω and S.

The energy before the impulse disturbance is observed during the first 0.1 s, then the impact furnishes energy to the beam, and the control damps the system during the next 2 s (−30 dB). The final level of energy is the same as the one before the impulse. It can be noticed that the energy

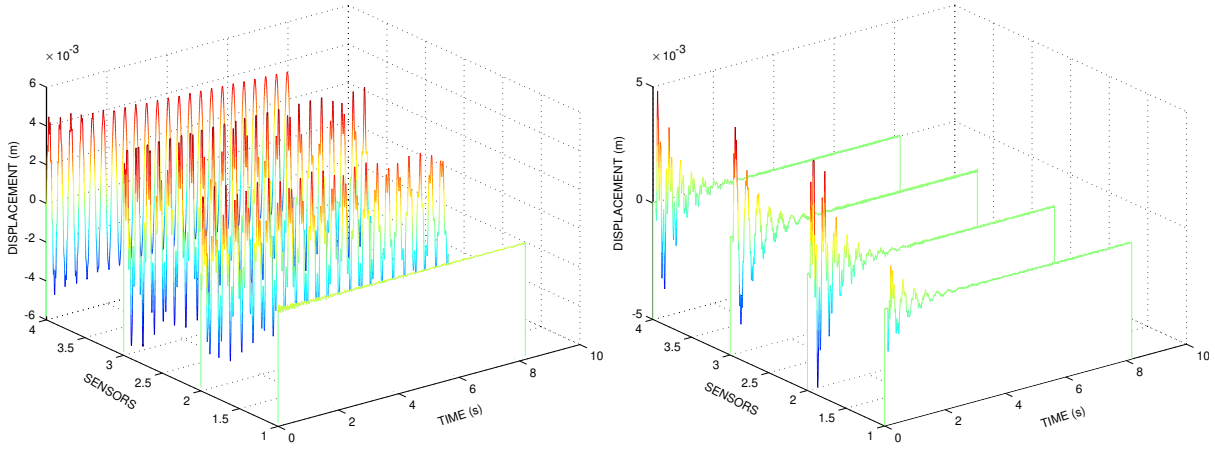

Fig. 10. Measured displacements with sensors 1,2,3 and imposed control after an impulse excitation given at $t = 0.1$ s, uncontrolled (left), controlled (right).

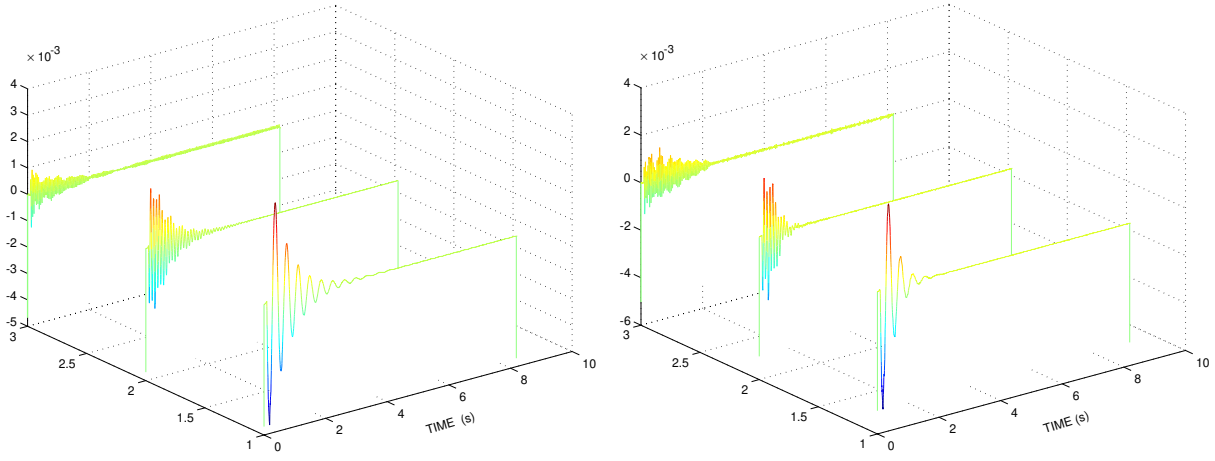

Fig. 11. Modal intensities of the controlled displacement, after an impulse excitation given at $t = 0.1$ s, left: with $\omega = 1$, $S = 30$ s, right: $\omega = 2$, $S = 30$ s.

Table 2
Modal parameters for different values of the control parameter ω

ω	Modes (Hz)	Frequencies (Hz)	Damping ratio (%)
0.5	1	3.2	3.3
	2	11.24	1.15
	3	23.7	0.4
1	1	3.1	6.1
	2	11.4	1.28
	3	23.5	0.54
2	1	3.06	9.5
	2	11.3	2.4
	3	23.62	0.15

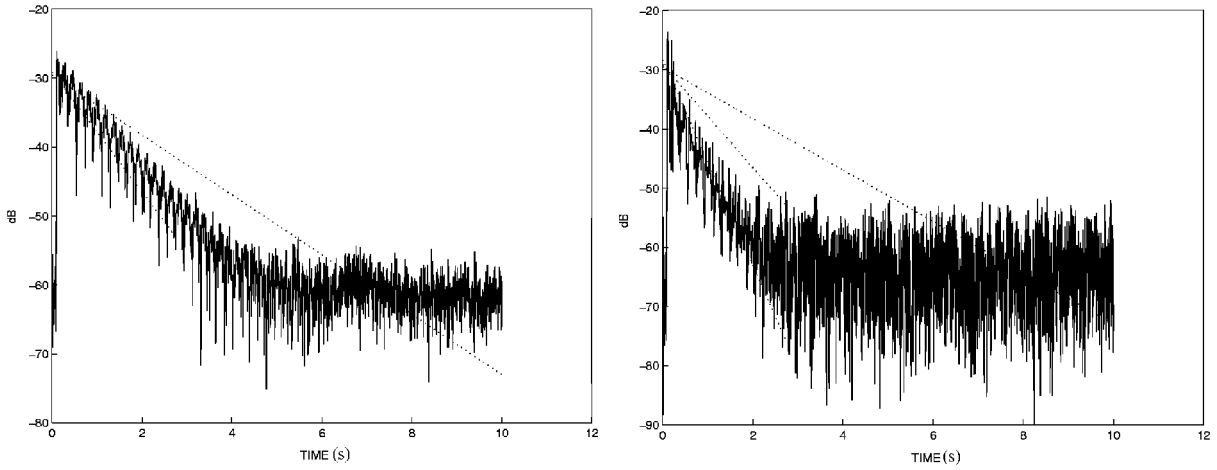

Fig. 12. *w-energy* of the controlled structure, with impulse excitation given at $t = 0.1$ s, left: $\omega = 0.5$, $S = 30$ s; right: $\omega = 1$, $S = 30$ s.

decays truly as $e^{-4\omega t}$. In both graphs $e^{-4\omega t}, e^{-2t}, e^{-t}$ are plotted in dotted lines. Again, the larger ω, the faster the decay of the response. The actual decay rate coincides with the theoretically expected one.

4.3. LQ results with exogeneous impulse disturbance

Here, $r = 5 \times 10^4$ is the smallest value of r before the spill-over instability occurs. Therefore this LQ control is the most efficient one for $\mathbf{Q} = \begin{bmatrix} diag(\lambda_i) & 0 \\ 0 & I \end{bmatrix}$. Fig. 13 shows the same results as before in the case of LQ strategy. See Figs. 10 and 11 for a comparison. Obviously this stabilization procedure is less efficient than Komornik's one.

Further comparison of Komornik's and LQ strategies involves the mechanical energy (see Fig. 14) $E_m(t) = \int_0^L 1/2\rho A(\partial y(x,t)/\partial t)^2 \, dx + \int_0^L 1/2EI(\partial^2 y/\partial x^2(x,t))^2 \, dx$ for both controlled beams. To compute this energy, the real displacement $y(x,t)$ is *now* discretized as $y^N(x,t) =$

$(1 - x/L)v(t) + \sum_{i=1}^{N} \bar{\alpha}_i(t)\theta_i(x)$, where the first term represents the static part of the movement. Then an estimation of the mechanical energy reads

$$\bar{E}_m(t) = \frac{1}{2}\sum_{i=1}^{3} \bar{\alpha}_i'(t)^2 + v'(t)\sum_{i=1}^{3} \bar{\alpha}_i'(t)\int_0^L \left(1 - \frac{x}{L}\right)\theta_i(x)\,\mathrm{d}x + \frac{\rho AL}{4}(v'(t))^2 + \frac{1}{2}\sum_{i=1}^{3} \lambda_i \bar{\alpha}_i(t)^2. \tag{20}$$

Remark. (i) That the definition of the approximate state has changed has no influence on the control design since the energy is computed off-line at a postprocessing stage.

(ii) Choosing the mechanical energy as a performance index proves very severe and even unfair for this version of Komornik's algorithm that is inherently designed to rather minimize a weak norm which is totally different from the mechanical energy that LQ strategy aims at minimizing. Let it be emphasized that the mechanical energy amplifies the high frequencies whereas the *w-energy* amplifies the low frequencies.

Nevertheless, the mechanical energy is plotted for LQ and Komornik's algorithms in the case of an impulse disturbance. The parameters are chosen to generate the most efficient LQ control for the experimental set-up considered. However, as shown in Fig. 14, for Komornik's control only 2 s are required to let the energy decrease by 30 dB, whereas the LQ control requires almost 10 s.

4.4. Comparison between Komornik's algorithm and other feedbacks

The goal of this section is to compare the main features of integral force feedback, direct velocity feedback, linear quadratic regulator, and Komornik's feedback.

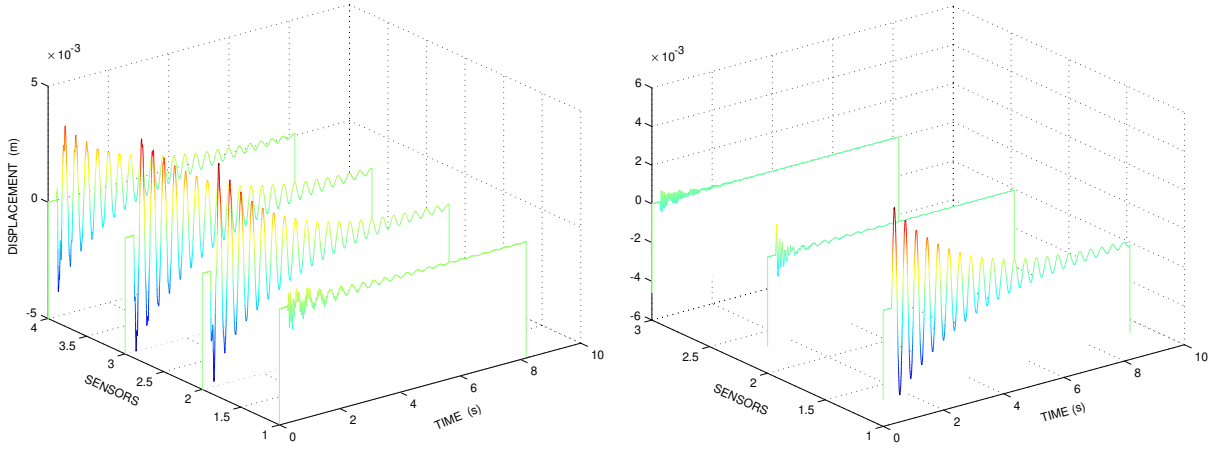

Fig. 13. LQ control for an impulse excitation given at $t = 0.1$ s; left: imposed displacement then sensors 1,2,3, right: modal displacement modal intensities 1,2,3.

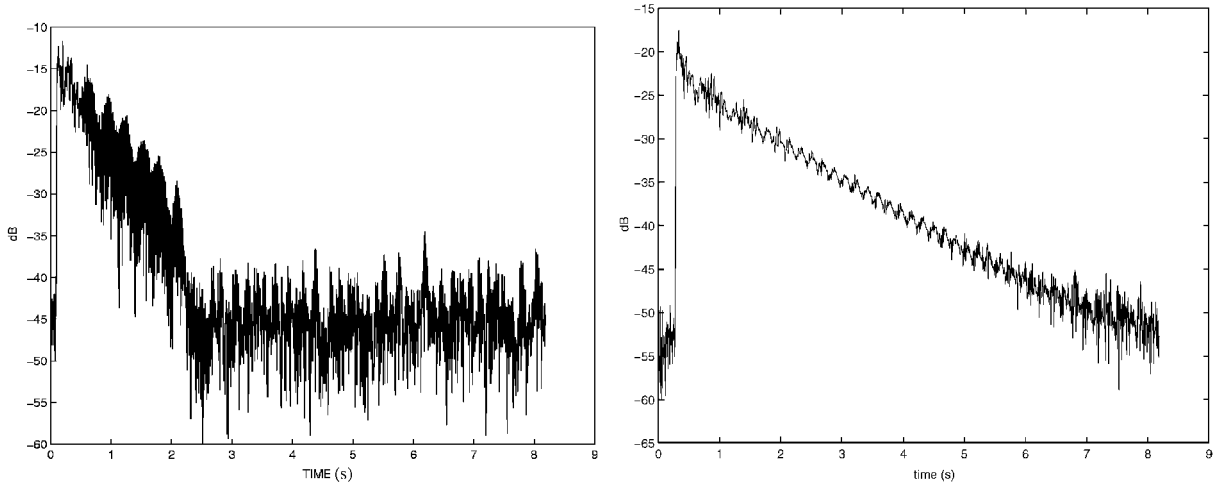

Fig. 14. Mechanical energy of the structure, with impulse excitation given at $t = 0.1$ s; left: Komornik's algorithm $\omega = 2$, right: LQ $r = 5 \times 10^4$.

- IFF, DVF: These strategies can be physically or numerically implemented without resorting to any model, although a model is definitely of interest for simulation purposes. In principle, these strategies are free of instability if no time delay is considered, but the necessary low- or high-pass filters as well as the dynamics of the sensors and actuators may introduce instabilities [2,43]. Moreover they are mostly effective close to the resonance frequency. The theoretical efficiency is bounded [3] and not uniform among the possible multiple modes to be damped simultaneously.
- LQ feedback: The advantage of that control is the minimization of control and state together. This global strategy attenuates all disturbances within a predefined bandwidth in a slightly damped system. However, instabilities due to spill-over may appear, due to the amplification of potential disturbances outside the frequency band of validity of the model. Except when special frequency-domain techniques apply, the classical LQ strategy requires the solution of an algebraic Riccati equation. A good approximation scheme that preserves the dynamics of the closed-loop system is thus needed, and this point remains partly open for the boundary control of an undamped wave or plate equation [8]. Recall [44,45] that standard discretization schemes can destroy the properties of the controlled system and thus fail to represent its real behaviour, even for a simple bar under traction and discretized by low-order finite elements: A general three-parameter method of approximation [27,34–37] however restores the stability and the convergence even when low-order finite elements are used. Moreover, a good Riccati solver is needed for the LQ synthesis and standard packages may not work well if the dimension of the system is too large (say $\geqslant 10$ states or five modes) or if the number of sensors differs from the number of actuators.
- Komornik's feedback: As optimal control, it features similar advantages and disadvantages as LQ feedback. The differences are the simpler software implementation and the better efficiency, at least when using boundary control. While the decay rate of IFF is limited by a maximum damping value, Komornik's feedback ensures an *arbitrarily large decay rate* in *w-energy*.

Moreover, the uniform stability of the control algorithm with respect to the number of modes [21] and to the discretization parameters holds for boundary control, in the absence of natural damping and for any kind of discretization tool, including low order finite elements. Furthermore, the implementation of Komornik's feedback does not involve the resolution of any Riccati equation although this is a particular LQ strategy, but rather the resolution of a simple non-singular linear system. Finally, a *single parameter*, which is the expected efficiency, needs to be tuned. The control algorithm proves thus very easy to use. The main disadvantage of this method, with respect to DVF of IFF only, remains the spill-over instability which occurs for large values of the parameter ω. This problem is studied and original tricks are under development. See Refs. [24,46] for preliminary results.

5. Analysis of the experimental results by using a complete electro-mechanical model

The previous section showed that instability occurs on the third mode when $\omega > 2.2$. This problem probably originates from the coupling between the actuator and the structure. In order to explain this interaction, the whole electro-mechanical model of the system described in Fig. 15 is simulated.

5.1. Electro-mechanical modelling

The mechanical equations describing the interaction of the beam and the actuator write

$$\begin{cases} \rho A \partial_{tt} y(x,t) + EI \partial_{xxxx} y(x,t) = 0, & [0,L] \times [0,T], \\ y(0,t) = v(t) = y_e(t), -EI \partial_{xxx} y(0,t) = F_p(t), & [0,T], \\ y(L,t) = \partial_{xx} y(0,t) = \partial_{xx} y(L,t) = 0, & [0,T], \\ y(x,0) = y^0(x), \partial_t y(x,0) = y^1(x), & [0,L], \end{cases} \tag{21}$$

$$M_e y_e''(t) + K_e y_e(t) = F_e(t) + F_p(t) \tag{22}$$

and

$$L_e I'(t) + R_e I(t) + B l y_e'(t) = V(t). \tag{23}$$

In these equations, M_e and K_e represent the moving mass of the shaker and the stiffness of its suspension respectively. Moreover, $y_e(t)$ stands for the displacement of the beam at $x = 0$, and F_p for the shear force at $x = 0$, whereas F_e corresponds to the electro-mechanical force, given by Laplace's law $F_e(t) = BlI(t)$, where B is the permanent magnetic field, l corresponds to the coil length and $I(t)$ denotes the electrical current in the coil. Finally, L_e, R_e and $V(t)$ stand for the coil inductance and resistance and for the imposed voltage respectively. In the previous developments the actual controlling displacement $y_e(t)$ was assumed to be proportional to $V(t)$, but this is not the case.

A full variational formulation of Eqs. (21)–(23), and a Galerkin approximation based on P modes of the simply supported beam, one static mode and one purely electric mode, result in a finite set of coupled equations modelling the electro-mechanical behaviour of the discrete system, where the modal intensities $\alpha_i(t)$, the end displacement $y_e(t)$ of the beam, and the electrical current

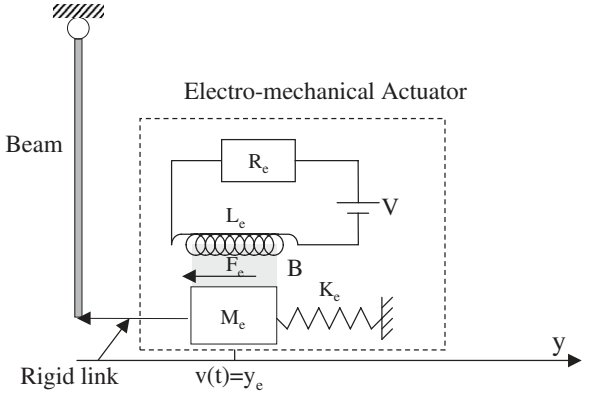

Fig. 15. Complete electro-mechanical system.

$I(t)$ can be chosen as primary unknowns:

$$\begin{cases} \alpha_i''(t) + z_i y_e''(t) + \lambda_i \alpha_i(t) = 0 \quad \text{for } i = 1, \ldots, P, \\ \left(M_e + \dfrac{\rho AL}{3}\right) y_e''(t) + \sum_{i=1}^{N} z_i \alpha_i''(t) + K_e y_e(t) - BlI(t) = 0, \\ L_e I'(t) + R_e I(t) + Bl y_e'(t) = V(t), \end{cases} \tag{24}$$

where $z_i = \int_0^L \rho A(1 - x/L)\theta_i(x)\,\mathrm{d}x$.

These equations differ from the ones obtained by applying the classical definition of the reaction force of the beam at its tip to the discretized displacement.

The parameters L_e, R_e, M_e, K_e and Bl are identified by means of the transfer function between the displacement $y_e(t)$ measured by a dedicated sensor and the imposed voltage $V(t)$, when the actuator is disconnected from the beam (Fig. 16). The theoretical transfer function reads

$$\frac{\tilde{y}_e}{\tilde{V}}(\omega) = \frac{Bl}{(M_e L_e (\mathrm{i}\omega)^3 + M_e R_e (\mathrm{i}\omega)^2 + \mathrm{i}\omega(L_e K_e + (Bl)^2) + K_e R_e)}. \tag{25}$$

A fitting technique leads to a rational function of $i\omega$ quite close to the measured transfer function (Fig. 16). Term by term identification yields four among the five unknown parameters, while R_e is directly measured on the system: $R_e = 2.5\ \Omega$, $L_e = 0.0069$ H, $M_e = 0.25$ kg, $K_e = 22800$ N/m and $Bl = 9.0429$ Tm. Fig. 17 shows the theoretical and measured transfer functions between $y_e(t)$ and $V(t)$ when the beam is connected to the actuator. The very good agreement between these curves confirms the quality of the identified model.

5.2. The complete electro-mechanical simulation of the control

The open loop electro-mechanical system described by Eq. (24) is closed by the feedback loop of the beam with ideal actuator. Mimicking the experiment, the first M modal participations are observed by means of Eq. (15), where the measured displacement is now built according to the

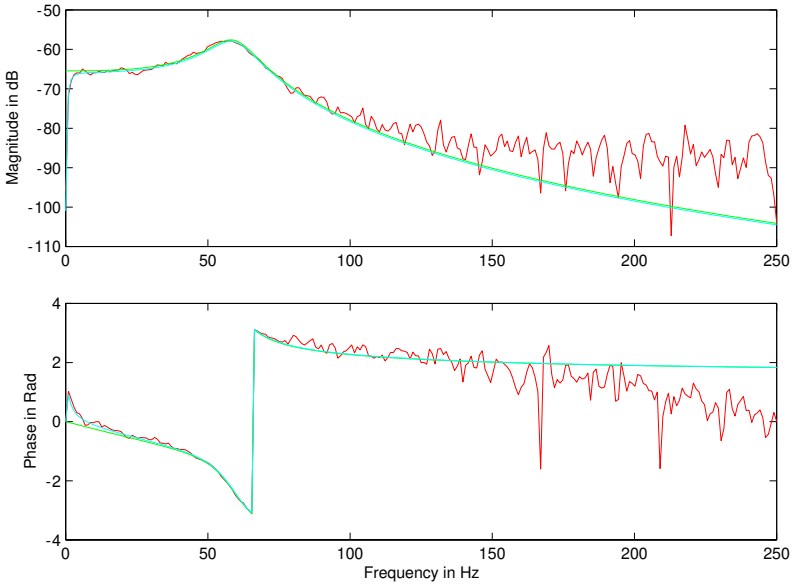

Fig. 16. The measured transfer function of the shaker: resulting displacement/input voltage and the corresponding fitting curve.

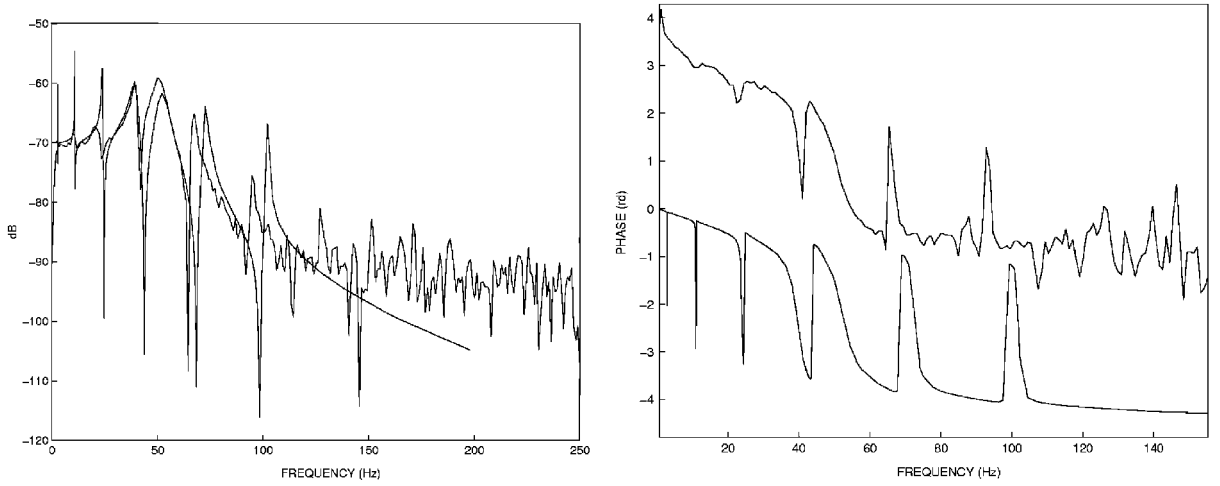

Fig. 17. Experimental and computed transfer function between $y_e(t)$ and $V(t)$ when the beam is connected to the actuator: left, the magnitudes in dB of each complex function; right: the phases with an artificial phase delay of π.

electro-mechanical model, that is to say $y(x,t) = \sum_{i=1}^{P} \alpha_i(t)\theta_i(x) + y_e(t)(1 - x/L)$ at every sensor location. Now the contributions of the $\mathrm{P}+2$ unknowns of model (24) may appear in $[\tilde{\alpha}(t)]_M$, causing observation spill-over. For the sake of simplicity, the dependence of $[\tilde{\alpha}(t)]_M$ with respect to P will be skipped in the sequel.

Moreover the filtered time-derivative of the generalized displacements, denoted by $\overline{\partial_t \bar{\alpha}_i}(t)$, is defined as the output $\dot{w}_i(t)$ of the state-space equation

$$\partial_t \begin{bmatrix} w_i(t) \\ \dot{w}_i(t) \end{bmatrix} = \begin{bmatrix} 0 & 1 \\ -2\xi_c\omega_c & -\omega_c^2 \end{bmatrix} \begin{bmatrix} w_i(t) \\ \dot{w}_i(t) \end{bmatrix} + \begin{bmatrix} 0 \\ \omega_c^2 \end{bmatrix} \bar{\alpha}_i(t),$$
$$w_i(0) = \dot{w}_i(0) = 0, \tag{26}$$

where $\omega_c = 2\pi.30$ and $\xi_c = 1/\sqrt{2}$. The discrete velocity estimator is implemented in the DSP as the solution of a recursive z-filter.

Hence, the control $v_M(t)$ to be applied is defined as in Eq. (17) by

$$v_M(t) = -[\mathbf{T}]_M[\mathbf{K}]_{M\times 2M}[[\bar{\boldsymbol{\alpha}}]_M(t),\ \overline{\partial_t[\bar{\boldsymbol{\alpha}}]_M}(t)]^t. \tag{27}$$

Finally, this control has to be imposed via the voltage $V(t)$ involved in Eq. (24). Let g denote the average of the inverse transfer function between $V(t)$ and $y_e(t)$ in the frequency band of interest, then set $V(t) = gv_M(t)$. This closes the system.

The gain g may look somewhat arbitrary, but the transfer function of the shaker disconnected from the beam proves relatively flat in the frequency band of interest (see Fig. 16).

It remains to plot (see Fig. 18) the pole locus of the closed-loop system as a function of ω. The choosen parameters are $M = 3$, $P = 6$ (there are $3 + 3$ residual modes taken into account).

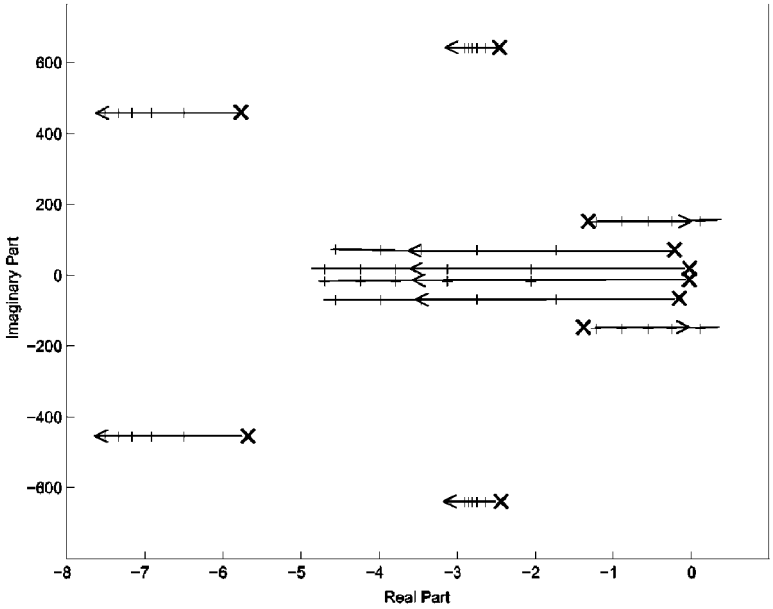

Fig. 18. The first five complex pole locus of the beam discretized with $N = 6$, $M = 3$, for control parameter $\omega = 1, 1.5, 1.8, 2, 2.2$.

From Fig. 18, it turns out that the third mode of the beam corresponding to the third plotted pole becomes unstable for $\omega = 2.2$. This purely numerical result coincides with the experimental observations since instability of the real system occurs for ω between 2 and 2.2. Thus, the complete model describing as accurately as possible the real implementation of the system in continuous time representation predicts the observed instability and the stability margin when the parameter ω varies. The third mode instability is induced by the electro-mechanical behaviour of the actuator coupled with the derivative low-pass filter used in the control feedback loop. Some solutions to this problem, in view of increasing stability and, so, the potential control efficiency are being explored.

6. Conclusions

A new strategy to stabilize flexible structures mainly due to Komornik has been tested experimentally. The algorithm has been described in detail for a simply supported beam. Then an approximate modal approach has been introduced in view of carrying out the experimental implementation. The classical LQ algorithm has also been implemented and compared to the new algorithm that exhibited much better stabilization performances. Energy attenuation exceeds 30 dB, stabilization is achieved 5 times faster than with LQ.

However, it is shown that increasing the control amplifies potential disturbances outside the considered frequency band, that is to say spill-over shows up for both algorithms. The contribution of the highest mode considered in the model is increased by the control and becomes unstable for a large value of the parameter ω. This problem is fully explained in the last section where a complete electro-mechanical model yields numerical results that perfectly match the experiments.

On the other hand, the control design based on the complete electro-mechanical model has not been undertaken.

Based on this experimental study the new feedback is shown:

(i) to be very efficient and to reject disturbances. It leads to a significant improvement of the stability of structures;

(ii) to be really simple to implement;

(iii) to generate the same spill-over as LQ;

(iv) to outperform the classical LQ feedback in this case.

Ongoing research aims at expanding the above results to the case of a larger frequency band and at engineering away spill-over by means of suitable mechanical formulations and feedback implementations. Extension to general systems in state-space form is also in progress from the computational viewpoint.

Appendix

The impact method [41,42] works as follows :

Let $\tilde{f}$ denote the Fourier transform of the function f. The theoretical transfer functions between the measured signals $y(x_k, t)$, $k \leqslant 3$, and the external load $F(t)$ collocated with sensor 1

at x_1 write

$$\begin{bmatrix} \tilde{y}(x_1,\omega) \\ \tilde{y}(x_2,\omega) \\ \tilde{y}(x_3,\omega) \end{bmatrix} = \begin{bmatrix} \sum_{i=1}^{\infty} \dfrac{\theta_i(x_1)\theta_i(x_1)}{\omega_i^2 - \omega^2 + 2i\xi_i\omega_i\omega} \\ \sum_{i=1}^{\infty} \dfrac{\theta_i(x_2)\theta_i(x_1)}{\omega_i^2 - \omega^2 + 2i\xi_i\omega_i\omega} \\ \sum_{i=1}^{\infty} \dfrac{\theta_i(x_3)\theta_i(x_1)}{\omega_i^2 - \omega^2 + 2i\xi_i\omega_i\omega} \end{bmatrix} \tilde{F}(\omega). \tag{A.1}$$

Remark. Damping terms are introduced in the transfer functions for several reasons : first, damping always shows up in any structure, and it is useful to identify it, no matter how small it is. Second, the method described hereafter yields damping for free. Third, a correct value of damping terms may help getting reliable values for other modal parameters. Finally, the small damping assumption must be substantiated by experiments.

The identification of most terms in Eq. (A.1) yields the modal parameters and the modal filter, made of the modal values at every sensor. Several steps are necessary:

Step 1: For a given impact at x_1, each time-varying signal is sampled with a frequency of 500 Hz for 10 s.

Step 2: A rectangular window is applied on the shock signal covering the useful part of these data in order to avoid the problems induced by the input noise. The measured signals given by the displacement sensors are multiplied by e^{-t/τ_c} in order to enforce the response signals to vanish before the end of the acquisition period of 10 s. The corresponding added damping ratio $(1/\tau_c)$ will be removed from the computed damping ratios at the end of the identification process.

Step 3: The FFT of above damped output signal is then divided by the FFT of the impact force signal, hence the transfer function.

Step 4: steps 1–3 are repeated 10 times. Then the average value of these 10 transfer functions is computed. Thus errors induced by the ouput noises are partly engineered away. Hence, an experimental realization $\bar{H}_k(\omega)$ of the exact transfer function between each sensor k and the impact force $H_k(\omega) = \sum_{i=1}^{+\infty} \theta_i(x_1)\theta_i(x_k)/(\omega_i^2 - \omega^2 + 2j\xi_i\omega_i\omega)$ is obtained.

Step 5: A rational fraction defined as

$$\hat{H}_k(\omega) = \sum_{i=1}^{3} \frac{R_{ki}}{(j\omega - p_i)} + \frac{\bar{R}_{ki}}{(j\omega - \bar{p}_i)} + \mathscr{E} \tag{A.2}$$

is fitted to each experimental transfer function $\bar{H}_k(\omega)$ obtained at Step 4.

Step 6: The modal parameters of the beam are identified by just comparing Eq. (A.2) with the close-form approximation of the exact transfer function

$$H_k(\omega) \approx \sum_{i=1}^{3} \frac{\theta_i(x_1)\theta_i(x_k)}{(\omega_i^2 - \omega^2 + 2j\xi_i\omega_i\omega)} + E \tag{A.3}$$

where the constant $E = \sum_{i=4}^{+\infty} \theta_i(x_1)\theta_i(x_k)/\omega_i^2$ accounts for the participation of the neglected modes. This identification leads to the system

$$\xi_i\omega_i + \mathrm{j}\omega_i\sqrt{1-\xi_i^2} = p_i, \quad \frac{\mathrm{j}\theta_i(x_1)\theta_i(x_k)}{2\omega_i\sqrt{1-\xi_i^2}} = R_{ki}, \quad E = \mathscr{E}. \tag{A.4}$$

The first set of equations yields the damping ratios and the frequencies. The collocated transfer functions, for $k = 1$, yield $\theta_i(x_1)$ for $i = 1, \ldots, 3$. The same equations then yield the non-collocated values $\theta_i(x_k)$, hence an approximation $\tilde{\mathbf{C}}_\mathbf{d}$ of the modal matrix $\mathbf{C}_\mathbf{d}$ introduced in (13), and an approximate filter by inversion.

References

[1] M.J. Balas, Direct velocity feedback control of large space structures, *Journal of Guidance and Control Engineering Notes* 2 (3) (1979) 252–253.

[2] Y. Achkire, A. Preumont, Active tendon control of cable-stayed bridges, *Journal of Earthquake Engineering and Structural Dynamics* 25 (1996) 585–597.

[3] A. Preumont, *Vibration Control of Structures: An Introduction*, Kluwer Academic Publishers, Dordrecht, 1997.

[4] J. Zabczyk, *Mathematical Control Theory: An Introduction*, Birkhauser, Boston, 1992.

[5] T.T. Soong, *Active Structural Control, Theory and Practice*, Longman, New York, 1990.

[6] H. Özbay, *Feedback Control Theory*, CRC Press, Boca Raton, FL, 2000.

[7] A. Emami-Naeini, G.F. Franklin, J.D. Powell, *Feedback Control of Dynamical Systems*, Addison-Wesley, Reading, MA, 1994.

[8] I. Lasiecka, R. Triggiani, *Differential and Algebraic Riccati Equations with Applications to Boundary/Point Control Problems: Continuous Theory and Approximation Theory*, Vol. 164, Springer, Berlin, 1991.

[9] M.J. Balas, Feedback control of flexible systems, *IEEE Transactions on Automatic Control* 23 (1978) 673–679.

[10] J.-L. Lions, Exact controllability, stabilization and perturbations for distributed systems, *SIAM Review* 30 (1988) 1–68.

[11] V. Komornik, Stabilisation frontière rapide de systèmes distribués linéaires, *Comptes Rendus de l' Académie des Sciences Paris, Série 1* 321 (1995) 433–437.

[12] V. Komornik, Rapid boundary stabilization of linear distributed systems, *SIAM Journal of Control and Optimization* 35 (5) (1997) 1591–1613.

[13] C. Bardos, G. Lebeau, J. Rauch, Sharp sufficient conditions for the observability, control and stabilization of waves from the boundary, *SIAM Journal of Control and Optimization* 30 (5) (1992) 1024–1065.

[14] S. Jaffard, Contrôle interne exact des vibrations d'une plaque rectangulaire, *Portugaliae Mathematica* 47 (4) (1990) 423–429.

[15] G. Lebeau, Contrôle de L'équation de Schrödinger, *Journal de Mathematiques Pures et Appliquées* 71 (1992) 267–291.

[16] G. Geymonat, P. Loreti, V. Valente, *Exact Controllability of a Shallow Shell Model*, International Series of Numerical Mathematics, Vol. 107, Birkhauser, Basel, 1992.

[17] V. Valente, B. Miara, Exact controllability of a Koiter shell by a boundary action, *Journal of Elasticity* 52 (3) (1999) 267–287.

[18] G. Leugering, J.E. Lagnese, E.J.P.G. Schmidt, *Modelling, Analysis, and Control of Dynamic Elastic Multi-link Structures*, Birkhauser, Boston, 1994.

[19] C. Bardos, T. Masrour, F. Tatout, Condition nécessaire et suffisante pour la contrôlabilité exacte et la stabilisation du problème de l'élastodynamique, *Comptes Rendus de l'Académie des Sciences Série 1* 320 (1995) 1279–1281.

[20] F. Bourquin, A numerical controllability test for distributed systems, *Journal of Structural Control* 2 (1995) 5–23.

[21] F. Bourquin, Approximation for the fast stabilization of the wave equation from the boundary, in: *Proceedings of MMAR2000*, Poland, August 2000.
[22] J. Lagnese, *Boundary Stabilization of Thin Plates*, SIAM Studies in Applied Mathematics, SIAM, Philadelphia, 1989.
[23] A. Benabdallah, M. Lenczner, Stabilisation de l'équation des ondes par un contrôle optimal distribué: estimation du taux de décroissance, *Comptes Rendus de l'Académie des Sciences Série 1* 319 (1994) 691–696.
[24] F. Bourquin, J-S. Briffaut, M. Collet, Smoothed fast stabilization, in: *Proceedings of the Second World Conference on Structural Control*, Kyoto, 1998.
[25] F. Bourquin, J-S. Briffaut, M. Collet, On the feedback stabilization: Komornik's method, in: *Proceedings of the Second International Symposium on Active Control in Mechanical Engineering*, Lyon, France, 1997.
[26] F. Bourquin, Numerical methods for the control of flexible structures: extended abstract of Briffaut's thesis, *Journal of Structural Control* 8 (1) (2001) 83–103.
[27] F. Bourquin, On the computation of b^*, in: *Proceedings of the European Meeting on Intelligent Systems*, *EMIS2001*, Ischia, Italy, September 2001.
[28] F. Bourquin, M. Collet, M. Joly, F. Lene, L. Ratier, An efficient control algorithm for beams: experimental results, in: *Proceedings of ACTIV1999*, Florida, December 1999.
[29] L. Ratier, Stabilisation Rapide des Structures et Mise en Oeuvre Experimentale, Ph.D. Thesis, ENS Cachan, France, 2000.
[30] J. Urquiza, Contrôle et Stabilisation des Structures Haubanees, Ph.D. Thesis, Université P. et M. Curie, Paris, France, 2000.
[31] J-S. Briffaut, Méthodes Numériques pour le Contrôle et Stabilisation Rapide des Structures, Ph.D. Thesis, Ecole Nationale des Ponts et Chaussées, Paris, 1999.
[32] D.L. Lukes, Stabilizability and optimal control, *Funkcial Ekvac* 11 (1968) 39–50.
[33] F. Allgower, T.A. Badgwell, J.S. Qin, J.B. Rawlings, S.J. Wright, *Nonlinear Predictive Control and Moving Horizon Estimation—An Introductory Overview*, Springer, Berlin, 1999, pp. 391–449.
[34] C. Bardos, F. Bourquin, G. Lebeau, Calcul de dérivées normales et méthode de galerkin appliquée au problème de la contrôlabilité exacte, *Comptes Rendus de l'Académie des Sciences Série 1* 313 (1991) 757–760.
[35] F. Bourquin, Approximation theory for the problem of exact controllability of the wave equation, in: *Proceedings of the Second SIAM Conference on Mathematical and Numerical Aspects of Wave Propagation*, Newark, DE SIAM, Paris, 1993, pp. 103–112.
[36] F. Bourquin, R. Namar, J. Urquiza, *Discretization of the Controllability Gramian in View of the Exact Boundary Control*: *the Case of Thin Plates*, International Series of Numerical Mathematics, Birkhauser, Basel, 1999.
[37] F. Bourquin, *Control of Flexible Structures: Control Theory and Approximation Issues*, CIMNE, Barcelona, 1998.
[38] M. Collet, Shape optimization of piezoelectric sensors dealing with spill-over instabilities, *IEEE Transactions on Control System Technology* 9 (4) (2001) 654–663.
[39] M. Collet, L. Jezequel, Active control with piezoelectric layers optimization, *Journal of Structural Control* 1 (1995) 59–79.
[40] K. Seto, *Lumped Modelling and Robust Control for Bridge Towers Under Construction*, CIMNE, Barcelona, 1992.
[41] D.J. Ewins, *Modal Testing: Theory and Practice*, Research Studies Press, Zetchwor, 1986.
[42] G. Kenneth, G. Mc Connel, *Vibration Testing: Theory and Practice*, Wiley Interscience, New York, 1995.
[43] G. Chamberland, Eléments de Contrôle Actif Non-lineaire. Théorie et Applications, Ph.D. Thesis, Ecole Centrale de Lyon, 2000.
[44] H.T. Banks, K. Ito, Y. Wang, Exponentially stable approximations of weakly damped wave equations, in: *Proceedings of the International Conference on Estimation and Control of Distributed Parameter Systems*, Vorau, Austria, 1991, pp. 1–33.
[45] J-A. Infante, E. Zuazua, Boundary observability for the space-discretizations of the 1-d wave equation, *Comptes Rendus de l'Académie des Sciences Serie 1* 326 (1998) 713–718.
[46] F. Bourquin, M. Collet, L. Ratier, Modelling and numerical issues for the control of flexible structures, in: G. Magonette, F. Casciati, (Eds.), *Proceedings of the Third International Workshop on Structural Control*, World Scientific, Singapore, 2000.